An inertial system for the production of electricity and hydrogen from sea wave energy

A. Colucci, V. Boscaino, G. Cipriani, D. Curto, V. Di Dio, V. Franzitta, M. Trapanese, A. Viola
DEIM, University of Palermo
Viale delle Scienze – building 9, 90128, Palermo, Italy
E-mail: mailto:Brandon.strong@teledyne.comeng.colucci@gmail.com, valeria.boscaino@unipa.it, giovanni.cipriani@unipa.it, domcurto@gmail.com, vincenzo.didio@unipa.it, vincenzo.franzitta@unipa.it, marco.trapanese@unipa.it, alessia.viola@unipa.it

***Abstract* — This paper aims at describing a small scale prototype of a complete wave energy converter system for hydrogen production promoting the opportunity of installation in Sicily, in the Mediterranean Sea. The opportunity to produce hydrogen from sea-water identifies ocean wave energy as the most promising solution for electricity generation including hydrogen production and storage. Even if hydrogen is considered one of the most promising secondary sources, criticism arises from both the academic and the industrial world mainly because hydrogen production requires electricity consumption. Furthermore, safety problems concerning hydrogen storage and transport are actually the main hindrance to full commercialization. In order to overcome production issues, hydrogen production and storage plants which are fully powered by renewable sources are continuously investigated. Advantages of the proposed system mainly rely on producing hydrogen by wave energy providing for on-board storage thus avoiding transport-related issues.**

Keywords — wave energy; inertial system; hydrogen

I. Introduction

Renewable sources are continuously promoted to reduce pollutant emissions [1]. Solar, wind and sea wave energy conversion are just a few examples. Hydrogen is actually considered one of the most promising secondary sources for a wide variety of applications ranging from automotive to household appliances. Criticism of hydrogen as a promising energy vector arises from both the academic and the industrial world mainly because hydrogen production requires electricity consumption. Furthermore, safety problems concerning hydrogen storage and transport are actually the main hindrance to full commercialization. In order to overcome production issues, hydrogen production and storage plants which are fully powered by renewable sources are continuously investigated. The chance of producing hydrogen from salt-water appoints ocean wave energy as the most promising solution for electricity generation including hydrogen production and storage. Wave energy devices need large investments of money throughout the device production phases. The current scenario with many concepts being patented in every country can be confusing; some technologies have the potential of being successful, whereas many others will not pass the concept level [2]. Assessing the effective degree of technological advancement of proposed solutions is fundamental to calibrate the state of art [3]. Although the sea can be considered an "infinite" resource of energy, the high cost of the design and realization of device is the main limit to the development of this new technology. This paper aims at describing a small scale prototype of a complete wave energy converter system for hydrogen production promoting the opportunity of installation in Sicily, in the Mediterranean Sea.

In the literature, wave energy converter devices are conventionally classified based on position, principle, size and orientation [3]–[6]. This first sorting is based on the position of devices in relation to the coastline. The first criterion is the distance of the wave energy converter to the shore resulting in onshore, near-shore and offshore devices. Following the working principle criteria, three main classes are distinguished: Overtopping Device, Oscillating Water Column, Wave Activated Bodies and Buoyant. The third type of classification is based on the capacity of devices to exploit wave energy in function of the ability to intercept the wave. Main requirements of wave energy converters (WECs) can be summed up: the WEC must be "storm proof" resisting to harsh weather conditions; extremely low environmental impact to surrounding ecosystem of the WEC; low-weight and low maintenance.

In the literature, the design of an efficient power equipment for wave energy systems is widely investigated. The main issue concerning the power electronics system relies in a finite length amplitude modulated characteristics of a sea wave burst clashing with a continuous supply requirement of the load equipment. In the literature, several solutions have been presented. A comprehensive review of wave energy converters and power electronics solutions is reported in [6], [7]. Sometimes, predictive sea wave models are seldom implemented thus increasing the complexity of the control system not achieving satisfactory results. Frequently, a AC-DC and a DC-AC converter are efficiently designed, including a DC link control [8]. In the last few years, resonant rectifiers have been proposed to achieve a continuous supply [9].

In this paper, a small scale prototype of a wave energy converter including the buoyant electrical generator, the power electronics equipment and a sea water electrolyzer is proposed. The design criteria of each device are discussed. Experimental results on the laboratory prototypes of the linear generator and the salt water electrolyzer are presented. A cost-effective and efficient power electronics equipment is designed based on a passive rectifier and a voltage controlled DC-DC converter. An energy storage is connected to the intermediate DC bus and properly designed to accommodate for a continuous supply

978-0-933957-43-5 ©2015 MTS

between consecutive bursts. Experimental waveforms on the linear generator have been imported in the circuit simulator to test the power electronics system as closely as possible to its effective behaviour. The system design criteria and simulation model are widely described. Simulation results on the power electronics equipment are shown to test the efficiency of the proposed solution.

II. Wave Characterization of the Mediterranean Sea

Different wave measuring network can report on the status of the sea that is known sites where the buoys are installed. Anyway the knowledge of the wave motion of big area outside of the measuring system is necessary to convert the mechanical energy in electric (energy) In particular, the most productive area, showing average values above 12 kW/m, is located in the western Mediterranean between the Balearic Islands and the western coast of Sardinia. The neighbouring region located in the Sicily channel, off the north-western and southern Sicilian coasts, is also very productive with an average wave energy flux per unit crest that reaches 9 kW/m. [5]. The north-western and southern coasts of Sicily have a lower potential with average wave power ranging between 2.5 and 6.5 kW/m. On the northern coast west of Palermo average wave power flux is between 4 and 5 kW/m gradually increasing to values between 5 and 6 kW/m between San Vito Lo Capo and Trapani. The most productive area is located along the coastal stretch that lies north of "Mazara del Vallo" where average power is above 6 kW/m reaching values around 7 kW/m near Favignana Island. The rest of the southern coast is the least productive with average power flux below 4.5 and as low as 2.5 kW/m. The only exception is the area between Punta Secca and Capo Passero where values are almost everywhere near 5 kW/m. Similarly to what was previously observed on the Sardinia coast there is a sharp decline in average power east of Palermo and north of Capo Passero [5].

An estimation of wave energy potential in Sicily was carried out by [10] using both buoy wave measurements from Rete Ondametrica Nazionale (RON), the Italian Government wave buoy network, and wave parameter data by ECMWF project European Centre for Medium-Range Weather Forecasts. Starting from these offshore and nearshore data, the presence of a "hot spot" site has been individuated to be a possible location for a wave energy farm, in particular to deployment the Traslator Wave energy devices proposed in this paper.

Hot spot is a term introduced by Iglesias and [11] to indicate a site with concentrated wave energy. The nearshore hot spots are often coastal areas that require coastal defence structures protecting the coasts from erosion caused by wave energy concentration, as numerous studies have demonstrated [12]–[16].

The three Sicilian coast side investigate by [10] are: coast near Capo Gallo (in front of Palermo), Mazara del Vallo, and Catania, respectively, on the north, east, and south coasts (Fig.1). The maximum wave power value (P_{max}), is at the Capo Gallo site (1240 $kW\ m^{-1}$), whereas the highest energy values are around at the Mazara del Vallo sites (41.97 and 31.50 $MWh\ m^{-1}$) (See Table 1)

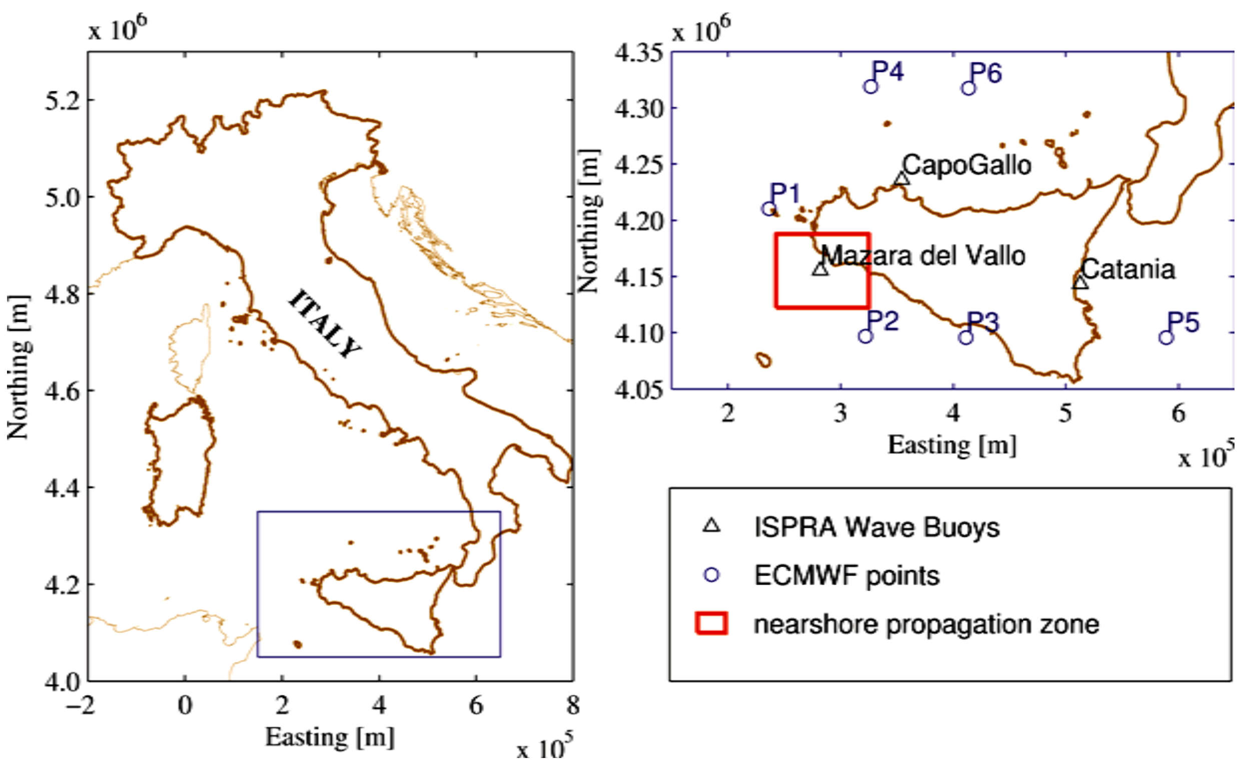

Fig.1 – Map of Italy and Sicily showing: 1) the location of ISPRA (RON) wave buoys and the ECMWF nodes considered and 2) the area examined for nearshore propagation (ED50-UTM33N) [10]

Sites	$H_{s,mean}$ $[m]$	$H_{s,std}$ $[m]$	$H_{s,max}$ $[m]$	P_{mean} $[kW\,m^{-1}]$	P_{max} $[kW\,m^{-1}]$	E_{annual} $[MWh\,m^{-1}]$
Capo Gallo	0.81	0.70	9.91	3.75	1240	21.20
Catania	0.63	0.55	6.20	1.76	188	13.34
Mazzara1	1.02	0.75	7.01	4.44	621	31.50
Mazzara2	1.02	0.77	6.67	4.86	200	41.97

Table 1 – Sea wave characterization of Hot Spot

III. MATHEMATICAL MODEL

This inertial system is made by an ellipsoidal floating buoy. It needs a mooring to keep its position on the sea surface. In this way all moving parts are carried in an hermetic vessel and the power generator is very reliable.

The inertial system needs several complex equations to describe its particular motion.

When a sea wave arrives, the buoy describes an angular oscillation around its center of gravity. The following equation describes the time trend of the angular oscillation (1):

$$I(t)\frac{\partial^2\vartheta}{\partial t^2} = M_{sea}(t) - m_r g l \sin\vartheta\,(t) \qquad (1)$$

In law (1) $I(t)$ is the **rotational inertia** of the buoy. This physical dimension changes in the time, due to the movement of the electric generator inside the buoy. $\vartheta(t)$ is the instant **angular rotation** measured from the **gravity vector** g. The physical dimension $M_{sea}(t)$ is the **moment (torque)** produced by the interaction between the sea wave and the buoy. m_r represents the **apparent mass** of the ballast, installed at the **distance** l from the gravity center of the system.

The apparent mass of ballast is given by law (2):

$$m_r = m\frac{\rho_{ballast} - \rho_{water}}{\rho_{ballast}} \qquad (2)$$

The equation (1) is a differential second order nonlinear equation with variable coefficients (see the $I(t)$ term). This equation is very complex to solve. As our goal is studying the electric generator, we will assume that the angular rotation follows the law (3):

$$\vartheta(t) = \vartheta_{max}\sin(\omega t) \qquad (3)$$

ϑ_{max} represents the **maximal value of the angular rotation** from the balance position; $\omega = 2\pi f$ is the **angular frequency** of sea wave.

The ϑ_{max} parameter can be measured during a fluid dynamics experiment in laboratory, using a test buoy.

If at the time t the angular position of the buoy is ϑ, the translator of the generator undergoes these following forces:

- $F_{g\vartheta}$ is the component of the **weight force** on the inclined plane;
- F_{fric} is the **friction force**, always directed in opposition to the motion of the translator;
- F_{cog} is the **cogging force**, created by the magnetic interaction between the magnets, installed on the translator, and the iron of the stator;
- F_{ele} is the **electric braking force**, created by generation of electric power;
- F_{spring} is the **spring force**.

If $r(t)$ is the the position of the translator barycenter at the time t, the movement of the translator is governed by the differential law (4):

$$F_{g\vartheta} - F_{fric} + F_{cog} - F_{ele} - F_{spring} = M_T\frac{d^2r}{dt^2} \qquad (4)$$

Each term of the law (4) can be estimated with a particular equation. The $F_{g\vartheta}$ force is given by the following law (5):

$$F_{g\vartheta} = -M_T g\sin[\vartheta(t)] \qquad (5)$$

The constant M_T is the **total mass** of the translator, including magnets and weights. $\sin[\vartheta(t)]$ is the sine function of the tilt angle, function of the time.

The friction force is given by law (6):

$$F_{fric} = \mathrm{sign}[v(t)]\ \mu M_T g\cos[\vartheta(t)] \qquad (6)$$

sign[v(t)] is the sign function, applied to the speed of the translator; μ is the coefficient of friction; $\cos[\vartheta(t)]$ is the cosine function of the tilt angle, function of the time. The constant μ can be measured in an experimental test.

The cogging force assumes averagely a null value. The real trend of this force can be estimated with a numerical finite element simulation. Usually this function can be approximated with a Fourier series, stopped at first harmonica:

$$F_{cogg} = C\sin[\psi r(t) + \varphi] \qquad (7)$$

The constant ψ is given by relation $\psi = 2\pi/\lambda$, where λ is the geometrical step, characterizing the magnetic phenomenon.

If the electric linear generator has a translator shorter than stator, the magnets will move only in the region of the stator. In this way cogging force assumes small value and has a geometrical step equal to range between two consecutive teeth of stator.

If instead the electric generator has a translator longer than stator, the magnets come in and out from the stator region. In this way cogging force is mainly generated by the end effect, id est the magnetic interaction between the first or the last tooth of stator and the magnet that enters or leaves the stator region. In this situation the λ dimension is equal to the range between two consecutive magnets.

The electrical braking force is caused by mechanical energy conversion into electrical This force is given by law (8):

$$F_{ele} = \frac{1}{v(t)} \sum_{K=1}^{3} i_K(t) V_{0K}(t) \qquad (8)$$

In (8) $v(t)$ is the **speed of the translator**; $i_K(t)$ is the **electrical current** that flows in the K-th winding; $V_{0K}(t)$ is **the induced voltage** generated inside the machine. This voltage is equal to the terminal voltage only in a test without electrical load.

The spring force is valuable with Hooke's law (9):

$$F_{ele} = -K_{spring}\left[r(t) - r_{rif}\right] \qquad (9)$$

K_{spring} is the **stiffness of the spring**; $r(t)$ is the linear position of the barycenter of the translator; r_{rif} is the linear position where the system is in the balance condition.

In the equation (8) was introduced the induced voltage. According to the linearity of derivative operation the Lentz law (10) can be written in a different form:

$$e(t) = -\frac{d\Phi_B}{dt} = -\frac{d\Phi_B}{dx}\frac{dx}{dt} = -v(t)\frac{d\Phi_B}{dx} = -v(t)F(x) \qquad (10)$$

$F(x)$ is function only of the translator position. This function can be defined, through numerical simulation or experimental test, performed under a uniform motion.

Using law (10), it is very simple calculate the induced voltage, because enough knowing only position $r(t)$ of the translator and its speed $v(t)$. Expressing $F(x)$ with a Fourier's series, stopped at third harmonic, and been the generator a three-phase machine, it is obtained law (11):

$$V_{0K}(t) = v(t)\left\{A_1 \sin\left[\psi r(t) + \varphi_1 + (2-K)\frac{2}{3}\pi\right] + A_3 \sin[3\psi r(t) + \varphi_3]\right\} \qquad (11)$$

A_1 and A_3 are the constants respectively of the first and the third harmonica; φ_1 and φ_3 are the corresponding phases.

In the end, the current that flows in K-th phase is given by law (12), assuming that the machine has resistive-inductive electrical circuit:

$$\frac{di_K}{dt} = \frac{1}{L_T}\left[V_{0K}(t) - i_K(t)R_T\right] \qquad (12)$$

The constants L_T and R_T are respectively the total inductance and resistance of the electrical circuit model.

IV. The Power Conversion System

The prototype is designed to produce electric energy and hydrogen from sea waves. Fig.2 shows the placement of the main components, installed inside the buoy:

- Electric power generator
- AC-DC converter
- Electrolyzer
- Hydrogen storage

Fig.3 is the external view of the power conversion system.

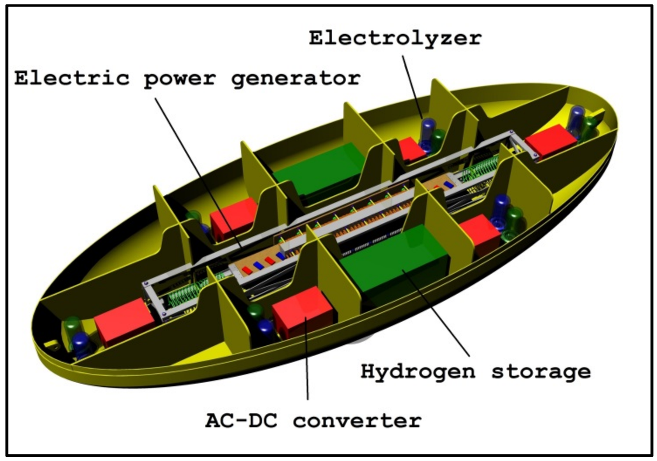

Fig.2 – Interval view of the Buoy

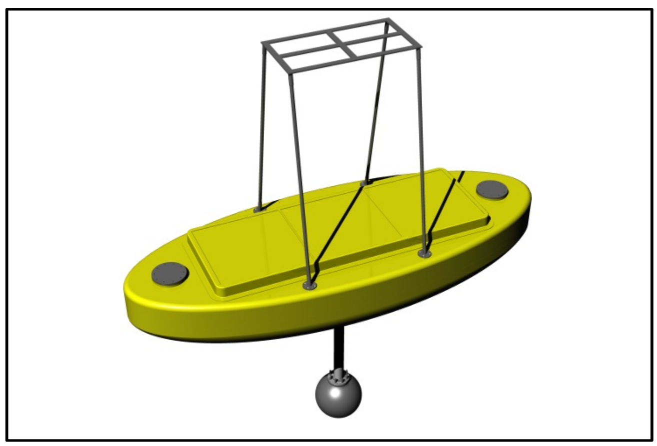

Fig.3 – External view of the buoy

A. Electric power generator

This electric power generator is a particular machine, defined as Permanent Magnet Linear Generator (PMLG). This device is available to convert directly the energy from oscillation of the buoy into electrical energy. According to authors' investigations, several advantages are brought by the installation of permanent magnets in the moving part of the machine. In this way, in fact, the magnetic induction field is generated without any current. In this solution conductors and sliding contacts can be avoided. Finally, Joule losses in the inductor are avoided.[17], [18]

The PMLG is composed by two parts: the **stator** and the **translator**. The first part is formed by two laminate iron blocks, therefore the PMLG is also a bilateral machine. The Fig.4 shows the details of the stator.

In each block of stator there are 126 iron sheets, having a thickness of 0.5 mm. The lamination is adopted to minimize the eddy currents. The geometric dimensions of each block are 972×60×65 mm. Each part of stator has 39 slots and 8 holes, with a diameter of 10.5 mm. The slots have two different widths: the first and last three have a width of 8 mm, while the other slots have a width of 12 mm. There are two different sizes because the smaller slots must contain only a winding, instead the others must contain two windings.

All the teeth have a width of 13.5 mm, except the first and last tooth that measure 7 mm.

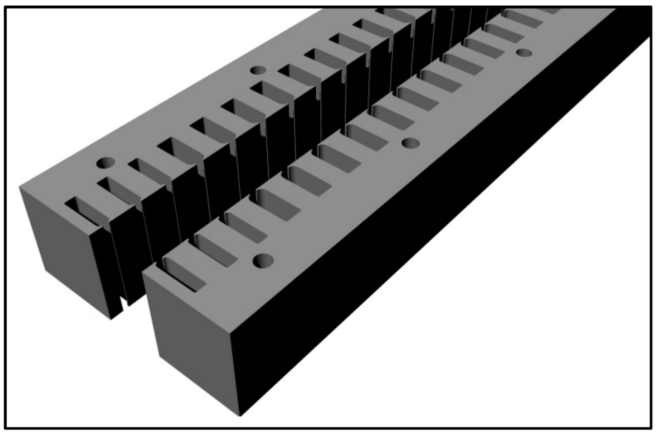

Fig.4 – Details of the iron stator

The machine is assembled using two tables of Bakelite, having the sizes 970×160×11 mm. Each table has 32 holes with a diameter of 10.5 mm. The holes are distributed in four lines. The external lines are required to make together the tables and the stator, using 16 threated rods The internal lines are required to install the rails of the translator.

In every block of the stator 36 windings are installed, each of which has 375 coils having a rectangular shape with average sizes of 85×135 mm. Each winding has a weight of 278 g and are realized in enameled copper wire of diameter 0.5 mm.

The translator is made assembling 40 Neodymium–Iron–Boron (Nd–Fe–B) permanent magnets on a Bakelite table, having sizes 1600×11×206 mm. The magnets have sizes of 60×30×15 mm, magnetization grade N40, a protective coating of Nickel (Ni-Cu-Ni) and a weight of 205.2 g. The magnetic pole is located in the larger surface. The magnets are installed in pairs along the translator, alternating the poles with a magnetic step of 76.2 mm, Fig.5a. The magnets are installed with a rotation angle of 17°, measured from the vertical direction, Fig.5b. This rotation is adopted to minimize the cogging force.

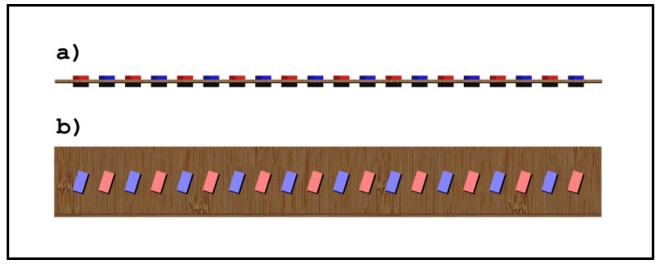

Fig.5 – Details of the Translator
a) Top view – b) Front view

Fig.6 shows the prototype of the permanent magnet generator after the assembling.

Fig.6 – The laboratory prototype of the Electric Generator

After several finite element simulations, the correct electric wiring is identified. The machine has six electrical phases that can be group in only three. In the first experimental test the six open circuit voltages are measured. The machine is tested using a constant force to move the translator. Being without any electrical load and ignoring the negligible cogging force, the translator moves uniformly accelerated linear motion. In the experimental test is measured an acceleration of $1.2\ \mathrm{m/s^2}$.

According to the Eq. (10) the six vacuum voltage can be evaluated with these following laws (13):

$$V_2(t) = \frac{at}{v_0}\left[A_1 \sin\left(\frac{\omega_0 a t^2}{2v_0} + \varphi_1\right) + A_3 \sin\left[3\frac{\omega_0 a t^2}{2v_0} + \varphi_3\right]\right]$$

$$V_4(t) = \frac{at}{v_0}\left[A_1 \sin\left(\frac{\omega_0 a t^2}{2v_0} + \varphi_1 - \frac{2}{3}\pi\right) + A_3 \sin\left[3\frac{\omega_0 a t^2}{2v_0} + \varphi_3\right]\right]$$

$$V_6(t) = \frac{at}{v_0}\left[A_1 \sin\left(\frac{\omega_0 a t^2}{2v_0} + \varphi_1 - \frac{4}{3}\pi\right) + A_3 \sin\left[3\frac{\omega_0 a t^2}{2v_0} + \varphi_3\right]\right]$$

$$V_1(t) = -V_4(t) \quad V_3(t) = -V_6(t) \quad V_5(t) = -V_2(t) \qquad (13)$$

where the parameters have the values in Table 2.

The experimental voltages are plotted in Fig.7. The theoretical voltages, according to laws (13), are plotted in Fig.8. By law (10) and laws (13), the voltages produced by generator are directly proportional to the speed of the translator. Since in a uniformly accelerated motion the speed increases linearly, likewise in the plots of vacuum voltages the maxima and the minima are located according to linear laws.

Quantity	Value	Quantity	Value
$\boldsymbol{A_1}$	$85.42\ [V]$	A_3	$28.81\ [V]$
$\boldsymbol{\varphi_1}$	$-0.8979\ [rad]$	φ_3	$0.4508\ [rad]$
$\boldsymbol{v_0}$	$1\ \left[\frac{m}{s}\right]$	ω_0	$41.233\ \left[\frac{rad}{s}\right]$

Table 2 – Values of the parameters

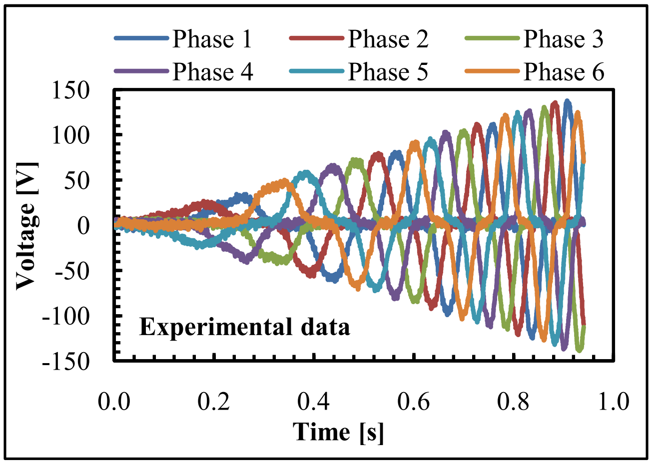

Fig.7 – Experimental open circuit voltages

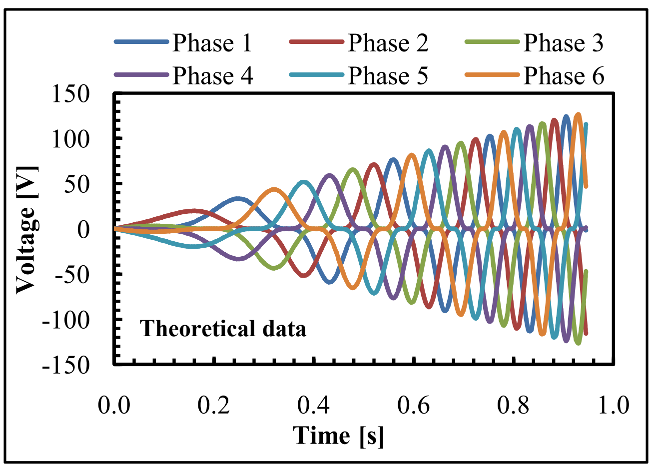

Fig.8 – Theoretical open circuit voltages

B. Electrolytic Stack

As shown in Fig.9, a laboratory prototype for sea-water electrolysis has been realized and tested. In this section, experimental results on the electrolyzer system are reported. Salt water has been used for experiments and hydrogen production has been highlighted by a small fuel cell stack directly fed from the electrolyzer. In Fig.9 measures on the laboratory prototype are reported.

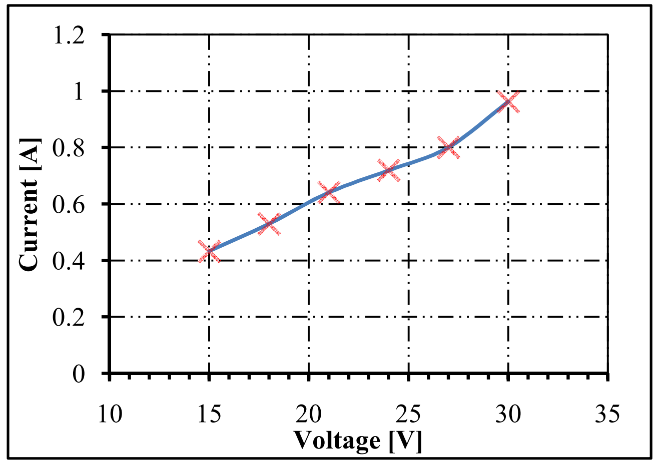

Fig.9 – Experimental results on the electrolyzer

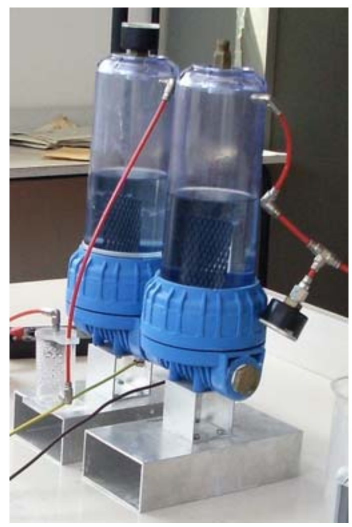

Fig.10 – The laboratory prototype of sea-water Electrolytic Stack and Hydrogen Storage

C. The power conversion system

In this paper, a low-cost power converter is designed and implemented. The converter is interposed between the linear generator and the electrolyzer. A small-scale prototype is designed and tested by simulation results concerning a single phase and a single electrolyzer cell. A modular architecture could be easily implemented by including all phases of the linear generator. The power conversion stage is designed to achieve a proper regulation of the output voltage which is the electrolyzer supply voltage. According to the experimental results on the sea-water electrolyzer prototype, the nominal output voltage is fixed at $20\ V$ and the minimum current is set at $0.2\ A$. According to the experimental results on the linear generator prototype, each generator phase supplies a voltage burst, as reported in Fig.11. The open circuit peak voltage is equal to $130\ V$ and the burst interval is equal to almost $1\ s$.

The power conversion stage is designed to achieve a continuous and regulated power supply to the electrolyzer within each wave burst. If the burst ends, the power converter will be supplied by a capacitive buffer. The capacitive storage element is properly designed to ensure a continuous supply of almost 2 s between two consecutive bursts.

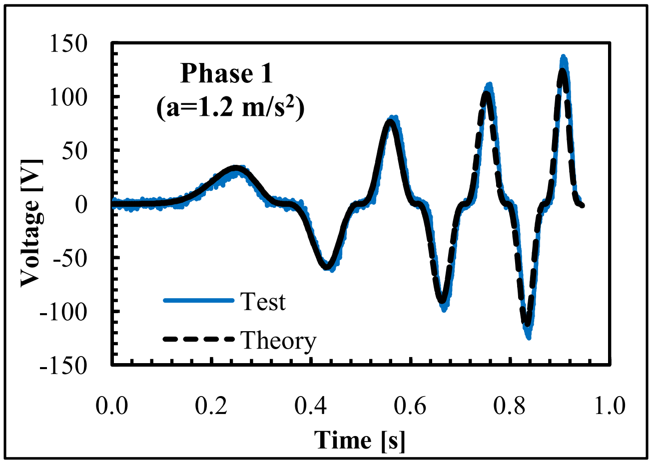

Fig.11 – Measured open-circuit voltage waveform generated by a single phase of six windings of the PMG

A diode bridge is designed as the front-end power converter. A buck-converter is cascaded to achieve control and regulation of the output voltage.

The supercapacitor is introduced at the output of the diode bridge in order to ensure a proper regulation even after the voltage burst. The supercapacitor could be placed at the output of the buck converter or at the output of the diode bridge. By introducing the storage buffer at the output of the diode bridge, a longer lasting self-supply is achieved between two consecutive bursts, mainly because the higher voltage at the common DC link. Because of the inductive behaviour of the generator, the supercapacitor value should be accurately designed to avoid any instability and oscillation at the intermediate DC link. Furthermore, the choice of the specific cascaded DC-DC converter is tied to the inductive behavior of the generator. Theoretically, a buck-boost topology should be designed to ensure a proper regulation over the whole burst interval. In fact, the burst voltage starts and ends at zero value. Yet, all input inductive DC-DC configurations must be discarded to avoid instabilities. A buck converter is selected. The supercapacitor could be designed to holds the DC voltage between each burst at an higher level than the output voltage. During the first burst, as it will be shown by simulation results, transients on the output voltage are highlighted due to the rising input voltage. As it will be shown by simulation results, a proper operation of the buck converter is ensured by slow time constants involved and by an accurate design of the control subsystem.

With regards to the storage element at the output of the diode bridge, the capacitor theoretically charges up to the burst peak of $130\,V$. Then, the storage element should supply the nominal power of $4\,W$ to the electrolyzer discharging towards the nominal voltage of $20\,V$. If the input voltage of the buck-converter drops below $20\,V$ the converter is disabled and the output storage element supplies the electrolyzer discharging toward zero value.

In order to design the C_{rect} capacitor, the following design relationship is considered:

$$P_{out}T_{out} = \Delta E_c = \frac{C_{rect}}{2}[V^2]_{20}^{30} \qquad (14)$$

From the (14), the capacitor value is fixed at 3.3 mF to achieve a 2.3 s self-supply interval. After 2.3 s, the buck converter will be disconnected. The output capacitor C_{out} will discharge at a constant current rate which is the electrolyzer current.

The buck converter is designed for a proper operation under the continuous conduction mode of operation to avoid the overload of the C_{rect} capacitor. The switching frequency is fixed at $100\,kHz$.

Continuous conduction mode condition is given by:

$$L > \frac{V_{out}(1-D)}{2f_{sw}I_0} \qquad (15)$$

If $D = D_{min}$ in (15), the worst-case condition will be accounted for. Over the whole operating range, the minimum duty-cycle value, corresponding to the maximum input voltage is equal to $15\,\%$. By limiting the inductor current ripple, the critical inductance value of $0.42\,mH$ is obtained and a 1mH inductance value is selected to achieve a maximum current ripple of $0.2\,A$.

The output capacitor is designed to solve the trade-off between the damping factor and the resonant frequency of the output filter. In order to limit over- and under-shoots of the output voltage under input transients, the optimal damping factor should be selected to overcome the 0.707 limit. A trade-off arises between the damping factor and the resonant frequency. Around the resonant frequency the maximum sharp phase roll-off occurs. Consequently, compensation issues arise from an extremely low resonant frequency. The damping factor is given by:

$$\xi = \frac{R_{tot}}{2}\sqrt{\frac{C_{out}}{L}} \qquad (16)$$

In order to avoid stability and compensation issues deriving from an extremely low resonant frequency, the C_{out} is fixed at 1 mF thus achieving a 0.4 open-loop damping factor. The simulation model of the power electronics equipment housed in a single module is shown in Fig.12.

The generator phase is modelled by a series connection of an inductance LMT and a resistor RMT. According to experimental results $LMT = 308\,mH$, $RMT = 37\,\Omega$. The measured open circuit voltage waveform is forced as the input voltage of the power converter stage by means of Look-up Table (LUT) block which is available in PSIM libraries. Commercial components are modelled for inductors and capacitors including parasitic elements.

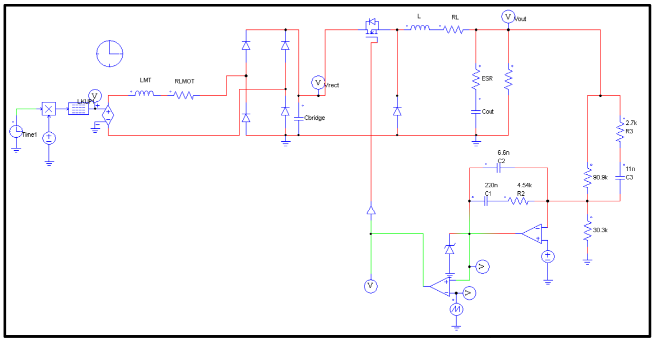

Fig.12 - Simulation model of the power electronics equipment.

The control network is designed to achieve proper regulation, adequate bandwidth and high suppression of input voltage transients. In Fig.14 Bode diagrams (magnitude and phase) of the open loop transfer function of the buck-converter at $V_{in} = 100\ V$ and $I_{load} = 0.2\ A$ conditions are plotted. As shown by Fig.14, the phase margin is not adequate to achieve a robust control.

A type III error amplifier is designed. In Fig.15 Bode diagrams (magnitude and phase) of the open loop transfer function including the error amplifier transfer function are plotted. Resistive parasitic elements are included. As shown by Fig.15, a phase margin of 62.7°, a gain margin of 31.1 dB and a 828 Hz bandwidth are achieved.

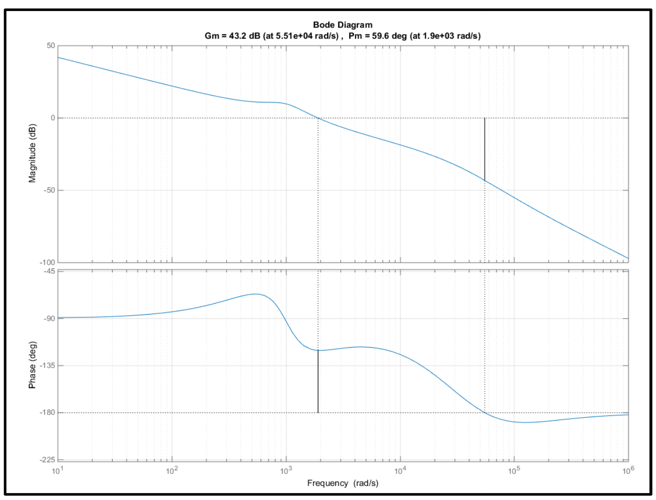

Fig.13 – Bode diagrams (magnitude and phase) of the open loop transfer function of the buck-converter at $V_{in} = 25\ V$ and $I_{load} = 0.2A$.

Performances are adequate to the specific application and a robust control against parameters and components tolerances is achieved. In order to test the robustness of the control subsystem against operating point changes, the analysis of system stability is carried out at several operating points.

In Fig.13, Bode diagrams of Bode diagrams (magnitude and phase) of the open loop transfer function including the error amplifier transfer function at $V_{in} = 25V$, $I_{load} = 0.2\ A$ are plotted. As shown, a phase margin of 59.6°, a gain margin of 43.2 dB and a 300 Hz bandwidth are achieved, confirming the robustness of the designed control system.

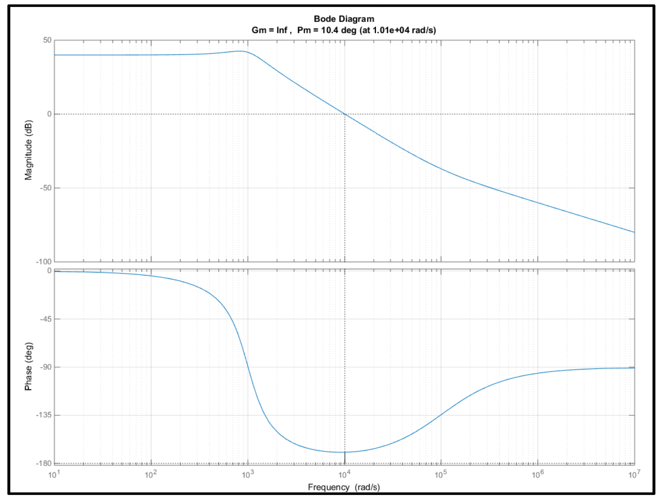

Fig.14 – Bode diagrams (magnitude and phase) of the open loop transfer function of the buck-converter at $V_{in} = 100\ V$ and $I_{load} = 0.2\ A$.

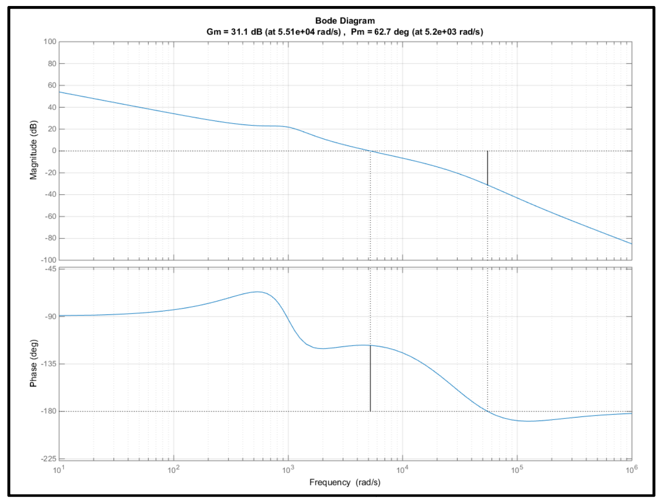

Fig.15 – Bode diagrams (magnitude and phase) of the open loop transfer function of the buck-converter at $V_{in} = 100\ V$ and $I_{load}\ = 0.2\ A$, including the type III error amplifier.

V. SIMULATION RESULTS

Simulation tests are carried out by forcing the measured open circuit voltage waveform as the input of the simulation model. In Fig.16, from the top to the bottom screen the electrolyzer supply voltage V_{out}, the diode bridge rectifier input voltage waveform $V_{in,rect}$ and the diode bridge rectifier output V_{rect} are shown. As shown by simulation results, a proper regulation of the electrolyzer supply voltage is achieved over the whole burst interval. The simulation starts at zero-voltage condition for each capacitive element. Therefore, the system start-up condition is emulated and simulated. At the beginning of the voltage burst, the input rectifier voltage falls below the nominal supply voltage value of 20 V and therefore a transient on the output voltage occurs. Yet, thanks to a proper and accurate design of the buck converter stage, the maximum voltage change under this extreme input transient is equal to 3 V. After the voltage burst peak, the rectifier output voltage follows a slow discharge of the capacitive buffer and the buck converter is supplied by the storage element. The system is simulated as closely as possible to its effective behaviour, including measured voltage waveforms and parasitic elements of commercial components. As shown by simulation results, under the whole voltage burst a proper regulation of the electrolyzer supply is achieved.

In Fig.17, a detail of the voltage waveforms of Fig.16 is shown. Notwithstanding voltage transients at the input of the buck converter, the maximum voltage change at the electrolyzer section is limited to 0.2 V corresponding to the 1% of the nominal voltage value.

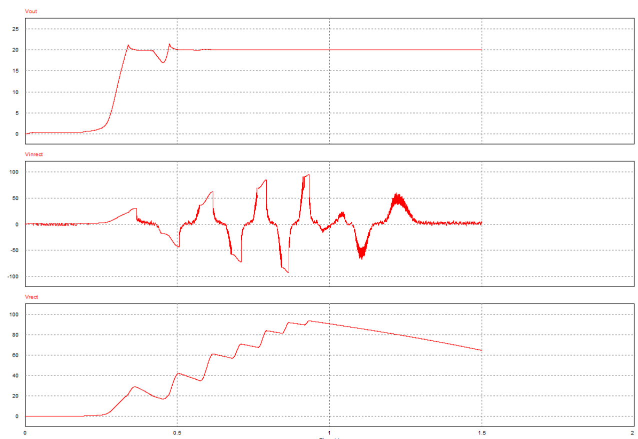

Fig.16 – Simulation results under an emulated sea-wave burst.

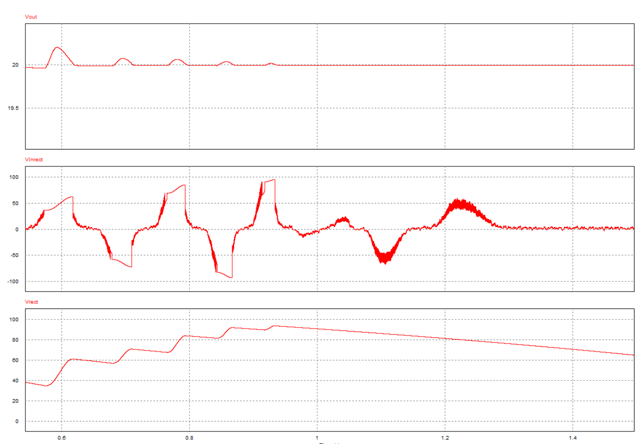

Fig.17 – A detail of simulation results under an emulated sea-wave burst

VI. CONCLUSION

In this paper, a small-scale prototype of a sea wave generator has been presented. This machine can produce electric energy and also hydrogen, from the renewable energy of the sea waves. The hydrogen production can be an important way to reduce the problem of pollution, produced by road transport.

The energy potential of sea waves is enormous, so the development of this technology is very important for the future.

The inertial prototype, analyzed in this paper, has the benefit of a simple structure, without any moving part exposed to the sea. This configuration ensures a greater reliability than other systems, with motive parts exposed to sea.

The electric power generator converts directly the wave energy into electrical. In this way the prototype has high electrical conversion efficiency. It is easy changing the scale of the system. It is also possible to produce a bigger buoy in which can be installed more than one electric power generator. In this way the project and building costs are minimized.

This system, through the use of Neodymium permanent magnets, is more compact than other similar technologies. According to our experimental tests, the prototype analyzed can produce 1 kW of electrical power, working at full load.

VII. REFERENCES

[1] B. Sørensen, *Renewable Energy - Its physics, engineering, environmental impacts, economics & planning*, 3rd ed. Elsevier Science, 2004.

[2] W. Sheng, R. Alcorn, and A. Lewis, “On improving wave energy conversion , part I□: Optimal and control technologies,” *Renew. Energy*, vol. 75, pp. 922–934, 2015.

[3] A. F. D. O. Falcão, “Wave energy utilization: A review of the technologies,” *Renew. Sustain. Energy Rev.*, vol. 14, no. 3, pp. 899–918, Apr. 2010.

[4] M. Trapanese, “Optimization of a sea wave energy harvesting electromagnetic device,” *IEEE Trans. Magn.*, vol. 44, no. 11 PART 2, pp. 4365–4368, 2008.

[5] L. Liberti, A. Carillo, and G. Sannino, “Wave energy resource assessment in the Mediterranean, the Italian perspective,” *Renew. Energy*, vol. 50, pp. 938–949, 2013.

[6] K. H. Mohamed, N. C. Sahoo, and T. B. Ibrahim, “A survey of technologies used in wave energy conversion systems,” *Proc. - 2011 Int. Conf. Energy, Autom. Signal, ICEAS - 2011*, pp. 594–599, 2011.

[7] Y. Hong, R. Waters, C. Boström, M. Eriksson, J. Engström, and M. Leijon, “Review on electrical control strategies for wave energy converting systems,” *Renew. Sustain. Energy Rev.*, vol. 31, pp. 329–342, 2014.

[8] V. Kurupath, R. Ekström, and M. Leijon, “Optimal constant dc link voltage operation of awave energy converter,” *Energies*, vol. 6, no. 4, pp. 1993–2006, 2013.

[9] C. Bostrom, B. Ekergard, R. Waters, M. Eriksson, and M. Leijon, “Linear generator connected to a resonance-rectifier circuit,” *IEEE J. Ocean. Eng.*, vol. 38, no. 2, pp. 255–262, 2013.

[10] M. Monteforte, C. Lo Re, and G. B. Ferreri, “Wave energy assessment in Sicily (Italy),” *Renew. Energy*, vol. 78, no. August, pp. 276–287, Jun. 2015.

[11] G. Iglesias and R. Carballo, “Wave energy and nearshore hot spots: The case of the SE Bay of Biscay,” *Renew. Energy*, vol. 35, no. 11, pp. 2490–2500, Nov. 2010.

[12] R. Carballo and G. Iglesias, “Wave farm impact based on realistic wave-WEC interaction,” *Energy*, vol. 51, pp. 216–229, 2013.

[13] E. Rusu and C. Guedes Soares, “Coastal impact induced by a Pelamis wave farm operating in the Portuguese nearshore,” *Renew. Energy*, vol. 58, pp. 34–49, Oct. 2013.

[14] a. R. Bento, E. Rusu, P. Martinho, and C. Guedes Soares, “Assessment of the changes induced by a wave energy farm in the nearshore wave conditions,” *Comput. Geosci.*, vol. 71, pp. 50–61, Oct. 2014.

[15] J. Abanades, D. Greaves, and G. Iglesias, “Coastal defence through wave farms,” *Coast. Eng.*, vol. 91, pp. 299–307, Sep. 2014.

[16] J. Abanades, D. Greaves, and G. Iglesias, “Wave farm impact on the beach profile: A case study,” *Coast. Eng.*, vol. 86, pp. 36–44, 2014.

[17] M. Trapanese, V. Franzitta, and A. Viola, “Design and Performance of a High Temperature Superconducting Axial Flux Generator,” *IEEE Trans. Magn.*, vol. 49, no. 7, pp. 4113–4115, Jul. 2013.

[18] V. Di Dio, V. Franzitta, D. Milone, S. Pitruzzella, M. Trapanese, and A. Viola, “Design of Bilateral Switched Reluctance Linear Generator to Convert Wave Energy: Case Study in Sicily,” *Adv. Mater. Res.*, vol. 860–863, pp. 1694–1698, Dec. 2013.